Synthesis, characterization and applications of WO$_3$:Eu as a new photocatalyst for dye removal of colored wastewater

Mohammad Ebrahim Olya[a,*], Leila Montazerghaem[a], Alireza Naeimi[b]

[a]Department of Environmental Research, Institute for Color Science and Technology, P.O. Box: 16765-654, Tehran, Iran,
Tel. +98 021 22969771; Fax: +98 021 22947537; emails: olya-me@icrc.ac.ir (M.E. Olya),
leila.montazerghaem@gmail.com (L. Montazerghaem)
[b]Department of Nanomaterials and Nano coatings, Institute for Color Science and Technology, Tehran, Iran,
alireza.naeimi68@gmail.com

A B S T R A C T

Europium-doped WO$_3$ nanoparticles were synthesized by solution combustion method. The prepared sample was characterized by means of X-ray powder diffraction (XRD), scanning electron microscopy, and energy-dispersive X-ray spectroscopy. The XRD pattern of powder revealed the monoclinic crystal lattice of WO$_3$. The presence of 0.3 wt% of europium was confirmed by energy-dispersive spectroscopy analysis. The photocatalytic efficiency of WO$_3$:Eu was evaluated by the degradation of reactive blue 194 (diazo dye) aquatic solution under irradiation of UV light (253 nm).

Keywords: Wastewater treatment; Photocatalyst; Dye removal; WO$_3$; Combustion synthesis

1. Introduction

Wet dyeing processes in textile industry have converted it to one of the major water consumers [1,2]. Approximately 15% of the total dye consumed in dyeing processes enters the wastewater directly and is released in nature [1]. Most synthesized dyes are organic molecules with complex structure and good chemical stability and resistance to light [3]. Mineralization and single stage of organic matter removal from wastewater are advantages of advanced oxidation methods compared with conventional wastewater treatment methods such as coagulation, adsorption, and membrane separation [4]. Advanced oxidation processes are suitable methods for the oxidation of a wide range of organic contaminants [5,6]. The good performance of photocatalytic process in oxidation and mineralization of recalcitrant organic materials has improved it into one of the best methods for treatment of wastewater containing organic matter among advanced oxidation processes. For this purpose, different

semiconductors (TiO$_2$, ZnO, WO$_3$, Fe$_2$O$_3$, Bi$_2$O$_3$, SiO$_2$, CdS, and ZnS) are utilized in this process [6–9]. These oxides will have the best performance when they have the most effective surface. There is an enhancement in efficiency of these materials if they are utilized in nanoscale. Oxide nanoparticles have been synthesized with different methods, including coprecipitation [10], inoculation [11], hydrothermal [12], and solid state. The microwave-assisted solution combustion method is a rapid, simple method with low power consumption for the preparation of nanopowders [13]. Tungsten oxide is an n-type semiconductor with a wide range of band gap energy, different phases, and combinations such as WO$_3$, WO$_2$, and WO$_{3-x}$ that have new applications in various fields of technology like electrochromic, photochromic, and gas chromic and photocatalytic [14]. These properties have paved the way for the employment of these metal oxides in a variety of fields, including flat panel displays, smart windows, and gas sensors such as H$_2$, H$_2$S$_2$, NH$_3$, and NO$_x$ [15]. Among these metal oxides, tungsten trioxide is of utmost importance, and due to its physical and chemical properties, it is extensively applied as gas sensors, electrochromite, photocatalytic, and

* Corresponding author.

photoelectrochemical [16,17]. High degradation ability, simple preparation, non-toxicity, and sufficient stability in acidic condition are considered as the major advantages of inexpensive WO_3, which make it a good choice to utilize as a photocatlyst [18,19].

Solution combustion synthesis is the fast and simple method that provides the possibility of achieving tungsten oxide nanoparticles with a high effective surface. The final product can be in the form of porous foams or dense particles, depending on the type of synthesized material. The solution combustion synthesis results from nitrate resource reaction with one or more organic fuels [20]. External heat sources such as furnaces, microwaves, or direct flame can be utilized to start the reaction and supply the activation energy. In the microwave-assisted synthesis, thermal gradient direction will be from the inside of the primary cores to the outside; however, in the synthesis with furnace, the heating methods are from the surface to inside of particles. This will bring about the difference in particle morphology [21]. The photocatalytic properties of the semiconductor can improve by increasing the dopant.

In the present study, the photocatalytic properties of the tungsten oxide nanoparticles doped with europium are investigated.

2. Experimental setup

2.1. Synthesizes of photocatalyst

Eu-doped WO_3 was prepared by microwave-assisted solution combustion method through the use of citric acid as combustion fuel. Tungsten powder (Sigma-Aldrich, Germany) and europium oxide (Eu_2O_3; Merck, Germany) were used as precursor. In the first step, 3 g of tungsten powder were dissolved in 50 mL of hydrogen peroxide (37%; Merck, Germany) in a spontaneous reaction. The pH value of the solution was up to 1. For europium doping, 0.02 g of Eu_2O_3 was dissolved in 5 mL of nitric acid (65%) and added to the solution. Thereafter, 1.5 g citric acid was added to the solution in order to improve the combustion power. The final solution was heated to 80°C until the formation of yellow gel. The prepared gel was put in a microwave oven (900 W) for 5 min. Grinding the final porous product enables it to be used in the reactor.

2.2. Characterization of photocatalyst

Morphological and surface properties of photocatalyst were evaluated by means of scanning electron microscopy (SEM; LEO 1455 VP SEM). X-ray diffraction (XRD) pattern was carried out with a Cu Kα (λ = 1.54056 Å) radiation in diffraction angle (2θ) range of 10°–80° with a typical step size of 0.026° with equipment STOE Stadi P to identify crystalline phase. The elemental analysis of product was investigated by energy-dispersive X-ray spectroscopy (EDX) detector (MIRA model, TESCAN, Czech Republic). The UV–Vis spectrophotometry (CECIL, one beam) was utilized to determine the light absorbance of dye solution.

2.3. Photocatalytic experiments

The photocatalytic experiments were performed in an annular semibatch photoreactor with internal volume of

320 mL, which was equipped with a high pressure mercury lamp (51 W, 253.7 nm, Osram) in the middle of the reactor (Fig. 1). It is evident that the rate of reaction under visible light irradiation is by far lower than providing under UV light. It is the reason why industries, which consider time as a basic factor, almost always use the UV light instead of visible irradiation. Because of that, the experiments are performed under UV light irradiation in this study.

The pH values of dye solution were adjusted by use of HCl and NaOH. Degradation of reactive blue (RB) 194 (Fig. 2) under UV light was studied to estimate the photocatalytic activity of prepared samples. RB 194 is a water-soluble diazo dye with $C_{23}H_{22}ClN_{10}Na_5O_{19}S_6$ chemical structure and high acid and temperature stability (λ_{max} = 600 nm). This dye is commonly used for dyeing cotton, silk, and viscose.

Photo degradation of dye is calculated by the following equation:

$$\% \text{ Decolourization} = \frac{(A_0 - A)}{A_0} \times 100 \qquad (1)$$

where A_0 is the initial light absorbance, and A is the light absorbance of dye solution during the time of the reaction.
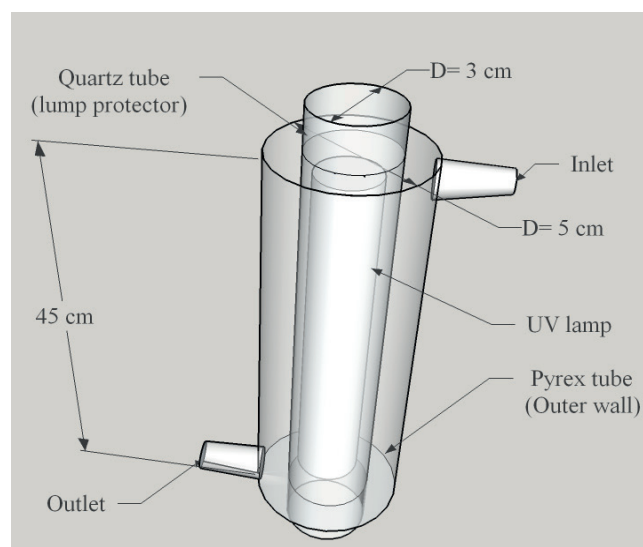
Fig. 1. Schematic illustration of photoreactor.
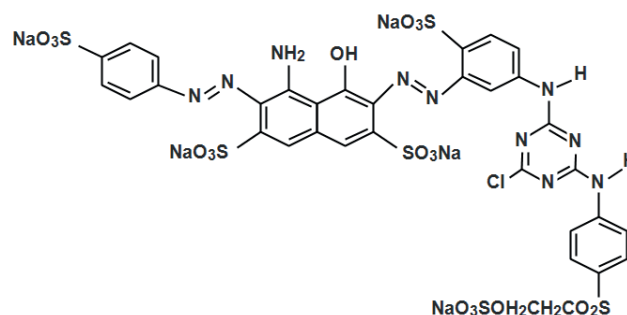
Fig. 2. Chemical structure of RB 194.

3. Results and discussion

3.1. Structural, morphological, and elemental properties of synthesized powder

Fig. 3 shows the result of XRD pattern of WO_3:Eu. The broad peaks of XRD pattern indicate the semiamorphous structure of synthesized catalysts, which is probably due to low temperature of combustion reaction. However, the main peaks [0 0 2], [0 2 0], [–2 0 2], [2 0 2], [2 2 2], [–4 0 2], and [3 4 0] demonstrate the conformity to monoclinic crystal structure (JCPDS No. 01-083-0951). The amount of up to 5 wt% of europium shows that there will be no peak, which corresponds to independent phase of europium in XRD pattern.

The result of SEM analysis in Fig. 4 shows the dense structure which is made up of masses of nanoparticles. Low intensity combustion and slow departure of gases arising from the burning of organic fuels such as CO_2 and nitrate gases lead to agglomeration of the particles to form the dense masses [22]. On the other hand, in this reaction, germination rate is higher than the cluster growing, which causes the formation of nanoparticles. High surface area of the formed masses is regarded as a positive parameter in decolorization processes.

Fig. 5 shows the EDX spectra of WO_3:Eu. The EDX analysis of three different points of powder surface indicated the uniform structure of prepared sample. Table 1 shows that W and O are the most common elements and are regarded as host compound by weight percentage of 84.8% and 11.1%, respectively. The successful doping of europium in host structure could be proved by EDX analysis result; weight percentage of europium as dopant element is 0.3 wt%. The existence of little amount of carbon on the surface of sample corresponds to combustion synthesis method.

3.2. Photocatalytic experiments

The photocatalytic activity of synthesized WO_3:Eu is evaluated by photodegradation of RB 194 aquatic solution under UV light irradiation. Wang et al. [23] prepared WO_3:Eu nanoparticle through a modified Pechini method and studied the photocatalytic performance of synthesized powder by photocatalytic degradation of Rhodamine B aquatic solution. The results show the expected performance of the photocatalyst.
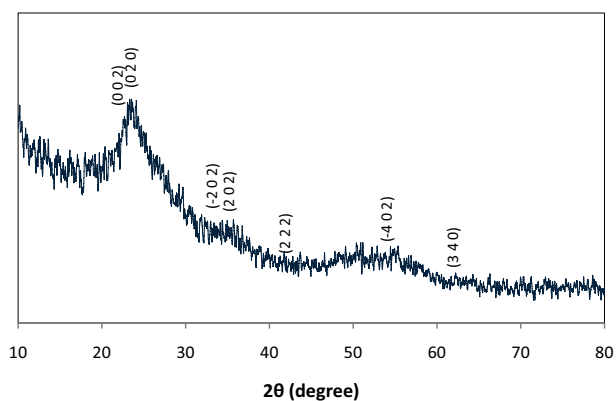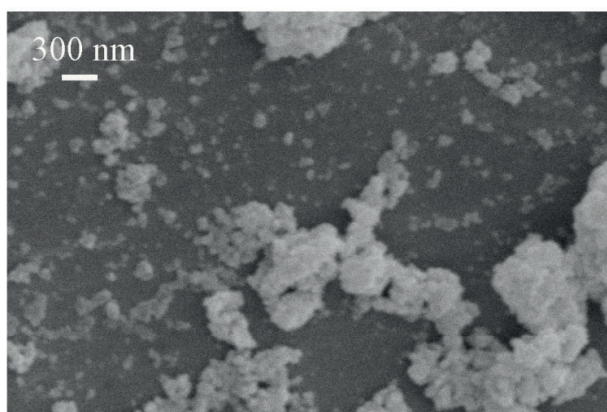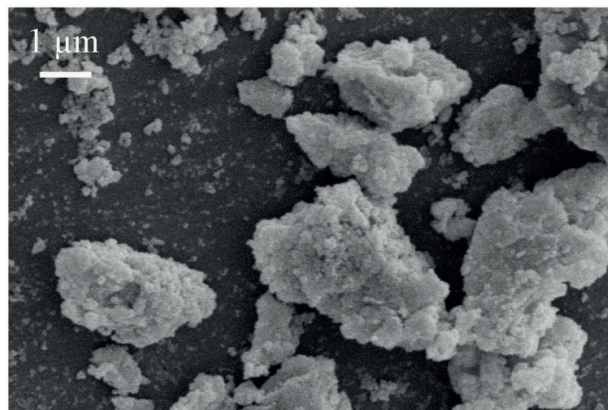
Fig. 4. SEM images of Eu-doped WO_3.
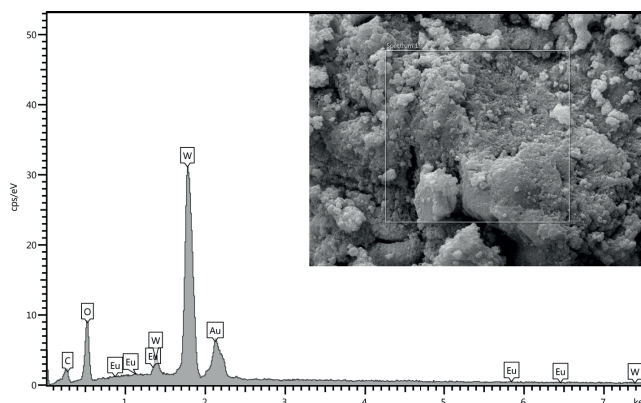
Fig. 5. EDX analysis of as-prepared sample.

Fig. 3. XRD pattern of WO_3:Eu.

Table 1
EDX elemental analysis of WO_3:Eu

	wt%	σ
W	84.8	0.7
O	11.1	0.3
C	3.7	0.3
Eu	0.3	0.7

In this study, the photocatalytic activity of Eu-doped WO$_3$ synthesized by solution combustion method was investigated for the first time. Operational parameter's effects comprising catalyst dosage, pH, and initial concentration of dye solution were investigated. Before the photocatalytic experiments, the samples were stirred in dye solution in the dark for 30 min in order to attain the adsorption–desorption equilibrium of dye molecules on catalysts surface. The results illustrate that there is a negligible dark adsorption in case of synthesized powder (below 5%).

3.2.1. Effect of catalyst dosage

The photocatalytic experiments involving five different dosages of catalyst for degradation of RB solution by initial concentration of 20 mg L^{-1} in 60 min reaction time under UV irradiation in order to investigate catalyst dosage were carried out. As illustrated in Fig. 6, maximum photocatalytic efficiency was achieved in 0.08 g L^{-1} catalysts dosage by 47.89% decolorization. The photodegradation was improved by increase in catalyst dosage from 0.02 to 0.08 g L^{-1}, which was due to increase in active sites of catalysts that contributed in the reaction. Increase in catalyst surface area leads to increase in $^\bullet$OH radical production and improve the photodegradation efficiency. Thereafter, increasing the catalysts dosage to more than 0.08 g L^{-1} causes light scattering and reduces the photons reaching the catalysts surface. On the other hand, agglomeration of catalysts occurs in higher catalyst dosages, which reduce the photocatalytic activity of the sample [7].

3.2.2. Influence of pH of dye solution

The pH of solution has a crucial effect on the efficiency of photodegradation of pollutants [24]. The effect of pH on photodegradation of RB was studied in the pH range of 3–9. Zero point charge of WO$_3$ is about 2.5 [25]; therefore, at higher pHs, the electrostatic repulsion between the negatively charged surface of catalyst and anionic dye prevents the adsorption of dye on photocatalyst surface and reduces the dye degradation efficiency[26]. On the other hand, the dissolution of catalyst in acidic solution leads to low removal efficiency at acidic pH range [27,28]. Fig. 7 shows that WO$_3$:Eu particle shows the best photocatalytic performance at natural pH (pH value of 6.7).

3.2.3. Effect of initial dye concentration

Initial dye concentration is one of the effective operational parameters on photodegradation of pollutant. At high concentrated dye solutions, dye adsorption on catalyst surface reduces the active sites of catalysts and prevents competitive adsorption of hydroxide ions on catalyst surface, which reduces the production of hydroxyl radical [26]. Thus, the dye degradation rate is reduced. On the other hand, photon adsorption by the dye molecules are another result of concentrated dye solution that prevents the photons from reaching the catalyst surface thereby reducing the rate of photoreaction [29]. Fig. 8 shows the reduction of dye degradation efficiency by increasing the initial dye concentration, which has been predicted.
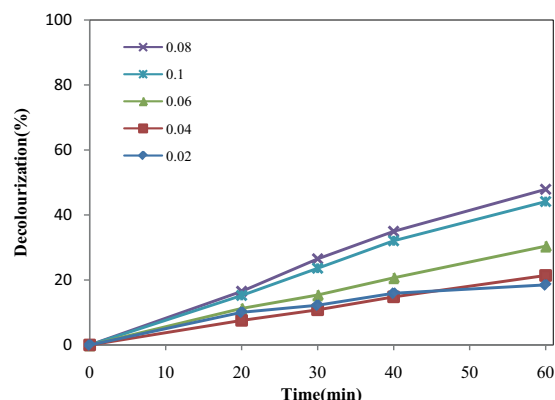
Fig. 6. Effect of photocatalyst dose on dye removal ([Dye]: 20 mg L^{-1}, reaction time: 60 min, pH: 7, and temprature: 23°C).
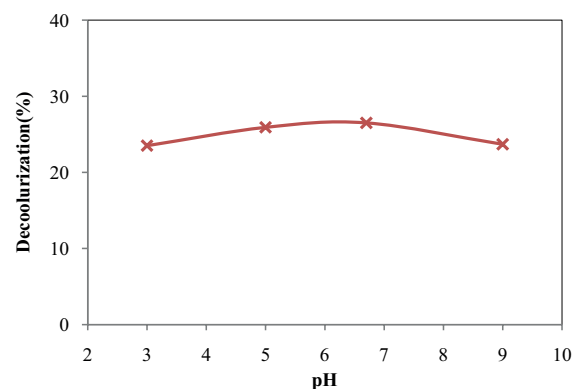
Fig. 7. Effect of pH of solution on dye degradation ([Dye]: 20 mg L^{-1}, reaction time: 60 min, and catalyst dose: 0.08 g L^{-1}).
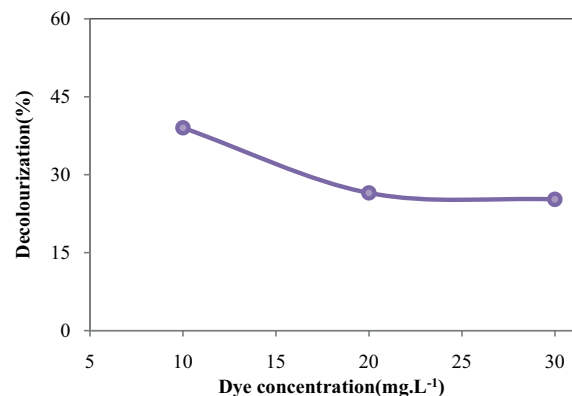
Fig. 8. Dependence of photocatalytic degradation of RB to initial dye concentration (catalyst dose: 0.08 g L^{-1}, pH: 7, and reaction time: 60 min).

The comparison of photocatalytic efficiency between the pure WO$_3$ and europium-doped WO$_3$ by catalyst loading of 0.08 g L^{-1}, toward degradation of 20 mg L^{-1} dye solution by natural pH is illustrated in Fig. 9. It is obvious that doping of europium to WO$_3$ molecules structures improved decolorization up to about 20%.

3.2.4. Probable photocatalytic mechanism

The WO$_3$:Eu was found to be more efficient than prepared WO$_3$ for degradation of RB dye under UV irradiation. Fig. 10 is considered as probable schematic diagram of photocatalytic mechanism of Eu-doped WO$_3$. Doping of catalyst prevents electron–hole recombination by trapping the induced electron in the following reactions:

$$Eu^{3+} + O_2^- \rightarrow Eu^{2+} + O_2 \tag{2}$$

$$Eu^{2+} + O_2 \rightarrow \bullet O_2^- + Eu^{3+} \tag{3}$$

When the UV light photons irradiate WO$_3$, a valence band electron is excited (Eq. (4)), and an electron–hole pair is produced:

$$WO_3 + h\nu \rightarrow WO_3 \left(h^+ + e^- \right) \tag{4}$$

The generated valence holes react with water and lead to the formation of $\bullet$OH radicals that could degrade the structure of the dye molecules (Eqs. (5)–(8)):

$$H_2O + h^+ \rightarrow H^+ + OH^- \tag{5}$$

$$h^+ + OH^- \rightarrow \bullet OH \tag{6}$$

$$R - H + \bullet OH \rightarrow \bullet R + H_2O \tag{7}$$

$$\bullet OH + Dye \rightarrow Degradation\ of\ dye \tag{8}$$

Conduction band electrons produce superoxide radical anions ($\bullet O^-$) by reacting with the adsorbed oxygen on catalyst surface. The created radical is efficient to degrade organic dyes (Eq. (9)) [27]:

$$O_2 + e^- \rightarrow \bullet O_2^- \tag{9}$$

4. Conclusion

Eu-doped WO$_3$ was synthesized by solution combustion method. The doping of europium has been revealed by EDX analysis. Existence of about 0.3 wt% europium has been shown in EDX elemental analysis. Formation of agglomerated nanoparticles masses has been shown in SEM images. The photocatalytic degradation of RB 194 under UV (UV-C) irradiation by pure and europium-doped WO$_3$ shows the improvement of dye photodegradation by doping of catalyst. The optimum pH and catalyst dosage for the photodegradation of 20 mg L^{-1} RB aquatic solution in a contact time of 60 min was found to be 6.7 and 0.08 g L^{-1}, respectively. Evaluation of initial dye concentration revealed that increasing dye concentration reduces the photodegradation rate.

	30 min	60 min
WO3	14.23	27.43
WO3/Eu	26.5	47.89

Fig. 9. A comparison between photocatalytic performance of pure WO$_3$ and Eu-doped WO$_3$ (catalyst dose: 0.08 g L^{-1}, [Dye]: 20 mg L^{-1}, contact time: 60 min, and temperature: 23°C).

Fig. 10. Probable mechanism of WO$_3$:Eu photocatalytic reaction.

References

[1] C.M. Teh, A.R. Mohamed, Roles of titanium dioxide and ion-doped titanium dioxide on photocatalytic degradation of organic pollutants (phenolic compounds and dyes) in aqueous solutions: a review, J. Alloys Compd., 509 (2011) 1648–1660.

[2] T. Robinson, G. McMullan, R. Marchant, P. Nigam, Remediation of dyes in textile effluent: a critical review on current treatment technologies with a proposed alternative, Bioresour. Technol., 77 (2001) 247–255.

[3] E. Forgacs, T. Cserhati, G. Oros, Removal of synthetic dyes from wastewaters: a review, Environ. Int., 30 (2004) 953–971.

[4] R. Marandi, M.E. Olya, B. Vahid, M. Khosravi, M. Hatami, Kinetic modeling of photocatalytic degradation of an azo dye using nano-TiO$_2$/polyester, Environ. Eng. Sci., 29 (2012) 957–963.

[5] F. Han, V.S.R. Kambala, M. Srinivasan, D. Rajarathnam, R. Naidu, Tailored titanium dioxide photocatalysts for the degradation of organic dyes in wastewater treatment: a review, Appl. Catal., A, 359 (2009) 25–40.

[6] M. Umar, H. Abdul, Adsorption Technique for the Removal of Organic Pollutants from Water and Wastewater, Chapter 8, M.N. Rashed, Ed., Organic Pollutants - Monitoring, Risk and Treatment, InTech, Croatia, 2013, pp. 195–208.

[7] T.A. Gad-Allah, S. Kato, S. Satokawa, T. Kojima, Treatment of synthetic dyes wastewater utilizing a magnetically separable photocatalyst (TiO$_2$/SiO$_2$/Fe$_3$O$_4$): parametric and kinetic studies, Desalination, 244 (2009) 1–11.

[8] C.-C. Liu, Y.-H. Hsieh, P.-F. Lai, C.-H. Li, C.-L. Kao, Photodegradation treatment of azo dye wastewater by UV/TiO process, Dyes Pigm., 68 (2006) 191–195.

[9] J. Zhang, Y. Hu, X. Jiang, S. Chen, S. Meng, X. Fu, Design of a direct Z-scheme photocatalyst: preparation and characterization of Bi$_2$O$_3$/g-C$_3$N$_4$ with high visible light activity, J. Hazard. Mater., 280 (2014) 713–722.

[10] M. Kahouli, A. Barhoumi, A. Bouzid, A. Al-Hajry, S. Guermazi, Structural and optical properties of ZnO nanoparticles
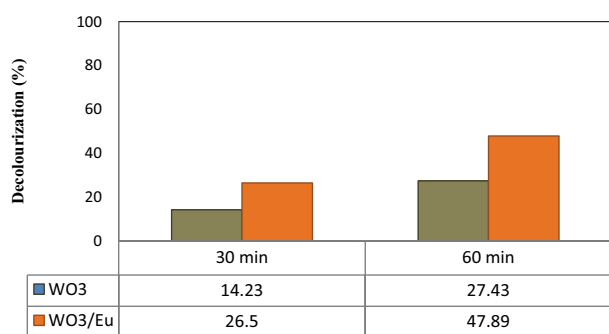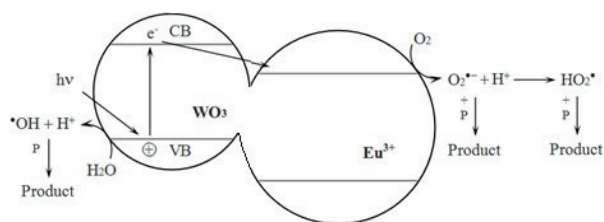
prepared by direct precipitation method: a review, Superlattices Microstruct., 85 (2015) 7–23.

[11] A.M. Motoc, I.A. Tudor, M. Petriceanu, V. Badilita, E.P. del Barrio, P. Jana, V. Fierro, A. Celzard, R.R. Piticescu, In-situ synthesis and attachment of colloidal ZnO nanoparticles inside porous carbon structures, Mater. Chem. Phys., 161 (2015) 219–227.

[12] M. Ahmadi, R. Younesi, M.J.-F. Guinel, Synthesis of tungsten oxide nanoparticles using a hydrothermal method at ambient pressure, J. Mater. Res., 29 (2014) 1424–1430.

[13] E.D. Sherly, J.J. Vijaya, Visible light induced photocatalytic degradation of 2,4-dichlorophenol on ZnO-NiO coupled metal oxides, Int. J. ChemTech Res., 7 (2015) 1369–1376.

[14] H. Zheng, J.Z. Ou, M.S. Strano, R.B. Kaner, A. Mitchell, K. Kalantar-zadeh, Nanostructured tungsten oxide – properties, synthesis, and applications, Adv. Funct. Mater., 21 (2011) 2175–2196.

[15] P. Huang, M.M. Kalyar, R.F. Webster, D. Cherns, M.N. Ashfold, Tungsten oxide nanorod growth by pulsed laser deposition: influence of substrate and process conditions, Nanoscale, 6 (2014) 13586–13597.

[16] R.F. Garcia-Sanchez, T. Ahmido, D. Casimir, S. Baliga, P. Misra, Thermal effects associated with the Raman spectroscopy of WO_3 gas-sensor materials, J. Phys. Chem. A, 117 (2013) 13825–13831.

[17] J.M. Wang, X.W. Sun, Z. Jiao, Application of nanostructures in electrochromic materials and devices: recent progress, Materials, 3 (2010) 5029–5053.

[18] H. Zhang, J. Yang, D. Li, W. Guo, Q. Qin, L. Zhu, W. Zheng, Template-free facile preparation of monoclinic WO_3 nanoplates and their high photocatalytic activities, Appl. Surf. Sci., 305 (2014) 274–280.

[19] D. Sánchez-Martínez, A. Martínez-de la Cruz, E. López-Cuéllar, Synthesis of WO_3 nanoparticles by citric acid-assisted precipitation and evaluation of their photocatalytic properties, Mater. Res. Bull., 48 (2013) 691–697.

[20] R. Ianos, R. Istratie, C. Pacurariu, R. Lazau, Solution combustion synthesis of strontium aluminate, $SrAl_2O_4$, powders: single-fuel *versus* fuel-mixture approach, Phys. Chem. Chem. Phys., 18 (2016) 1150–1157.

[21] R.V. Mangalaraja, S. Ananthakumar, Microwave Assisted Combustion (MAC) Synthesis of Mixed Oxide Electro-Ceramic Nanopowders, M. Lacknerq, Ed., Combustion Synthesis: Novel Routes to Novel Materials, Bentham Science Publishers Ltd., Austria, 2010, pp. 156–174.

[22] A. Alves, C.P. Bergmann, F.A. Berutti, Novel Synthesis and Characterization of Nanostructured Materials, Springer, Berlin, Heidelberg, 2013, pp. 11–22.

[23] C. Wang, X. Li, C. Feng, Y. Sun, G. Lu, Nanosheets assembled hierarchical flower-like WO_3 nanostructures: synthesis, characterization, and their gas sensing properties, Sens. Actuators, B, 210 (2015) 75–81.

[24] D. Rajamanickam, M. Shanthi, Solar light assisted photocatalytic mineralization of an azo dye, sunset yellow by using CAC/TiO_2 composite catalyst, Indian J. Chem., Sect A, 54 (2015) 613–618.

[25] M. ANIK, Anodic behavior of tungsten in H_3PO_4-K_2SO_4-H_2SO_4/ KOH solutions, Turk. J. Chem., 26 (2002) 915–924.

[26] I.K. Konstantinou, T.A. Albanis, TiO_2-assisted photocatalytic degradation of azo dyes in aqueous solution: kinetic and mechanistic investigations: a review, Appl. Catal., B, 49 (2004) 1–14.

[27] P.V. Korake, A.N. Kadam, K.M. Garadkar, Photocatalytic activity of Eu^{3+}-doped ZnO nanorods synthesized via microwave assisted technique, J. Rare Earths, 32 (2014) 306–313.

[28] B. Krishnakumar, B. Subash, M. Swaminathan, AgBr–ZnO – an efficient nano-photocatalyst for the mineralization of Acid Black 1 with UV light, Sep. Purif. Technol., 85 (2012) 35–44.

[29] N. Daneshvar, D. Salari, A.R. Khataee, Photocatalytic degradation of azo dye acid red 14 in water: investigation of the effect of operational parameters, J. Photochem. Photobiol., A, 157 (2003) 111–116.